




## An effective hybrid approach to remote-sensing image classification


Aravind Harikumar, Anil Kumar, Alfred Stein, P.L.N. Raju & Y.V.N. Krishna Murthy

To cite this article: Aravind Harikumar, Anil Kumar, Alfred Stein, P.L.N. Raju & Y.V.N. Krishna Murthy (2015) An effective hybrid approach to remote-sensing image classification, International Journal of Remote Sensing, 36:11, 2767-2785, DOI: [10.1080/01431161.2015.1047050](https://doi.org/10.1080/01431161.2015.1047050)

To link to this article: <https://doi.org/10.1080/01431161.2015.1047050>


 Published online: 21 May 2015.

 Submit your article to this journal [↗](#)

 Article views: 519

 View related articles [↗](#)

 View Crossmark data [↗](#)

 Citing articles: 1 View citing articles [↗](#)

## An effective hybrid approach to remote-sensing image classification

Aravind Harikumar<sup>a\*</sup>, Anil Kumar<sup>b</sup>, Alfred Stein<sup>c</sup>, P.L.N. Raju<sup>d</sup>, and  
Y.V.N. Krishna Murthy<sup>e</sup>

<sup>a</sup>Department of Geoinformatics, Indian Institute of Remote Sensing (IIRS), Dehradun, Uttarakhand 248001, India; <sup>b</sup>Photogrammetry and Remote Sensing Department, Indian Institute of Remote Sensing (IIRS), Dehradun, Uttarakhand 248001, India; <sup>c</sup>Department of Geoinformatics, ITC – Faculty of Geo-Information Science and Earth Observation, Enschede, The Netherlands; <sup>d</sup>Remote Sensing & Geoinformatics Group, Indian Institute of Remote Sensing (IIRS), Dehradun, Uttarakhand 248001, India; <sup>e</sup>Indian Institute of Remote Sensing (IIRS), Dehradun, Uttarakhand 248001, India

(Received 21 August 2014; accepted 12 March 2015)

This article presents a hybrid fuzzy classifier for effective land-use/land-cover (LULC) mapping. It discusses a Bayesian method of incorporating spatial contextual information into the fuzzy noise classifier (FNC). The FNC was chosen as it detects noise using spectral information more efficiently than its fuzzy counterparts. The spatial information at the level of the second-order pixel neighbourhood was modelled using Markov random fields (MRFs). Spatial contextual information was added to the MRF using different adaptive interaction functions. These help to avoid over-smoothing at the class boundaries. The hybrid classifier was applied to advanced wide-field sensor (AWiFS) and linear imaging self-scanning sensor-III (LISS-III) images from a rural area in India. Validation was done with a LISS-IV image from the same area. The highest increase in accuracy among the adaptive functions was 4.1% and 2.1% for AWiFS and LISS-III images, respectively. The paper concludes that incorporation of spatial contextual information into the fuzzy noise classifier helps in achieving a more realistic and accurate classification of satellite images.

### 1. Introduction

Image classification is widely applied in image analysis to extract land-use and land-cover (LULC) information from remote-sensing images. Conventional classification uses the spectral information from a single pixel (i.e. the digital number (DN) of the pixel). It is based upon the rather unrealistic assumption that pixels are pure (i.e. a pixel is the reflected value of a single class; Zhang and Foody 1998). In the 1980s, fuzzy classifiers were developed for addressing heterogeneity within a pixel, as a mixed pixel, thus improving the accuracy and making classification more realistic (Bezdek, Ehrlich, and Full 1984). Fuzzy classifiers generate fractional images (i.e. one image for every class, representing the associated membership values at the pixel level). Fuzzy c-means (FCM) classification is a popular fuzzy classification technique based on fuzzy set theory (Zadeh 1965). It is, however, sensitive to noise and outliers due to the probabilistic constraint involved (Krishnapuram and Keller 1993). Possibilistic c-means (PCM) classification addresses this sensitivity problem by redefining the concept of membership values. Membership values generated by a PCM classification represent the degree of

---

\*Corresponding author. Email: [aravind.harikumar@unitn.it](mailto:aravind.harikumar@unitn.it)

belongingness of a pixel to a class, rather than the degree of sharing of classes within a pixel as was the case with FCM. For this reason, PCM performs better in the presence of noise and outliers (Krishnapuram and Keller 1996).

Noise in remote-sensing images arises due to sensor deficiencies, data processing errors, atmospheric noise, and the presence of classes other than the class of interest. The presence of such noise in a remote-sensing image degrades the classification accuracy. Noise clustering (NC) is robust against noisy data and has been used successfully in various fields (Dave' 1991). It groups all noisy pixels into a separate class called the noise class based on their spectral properties. Image noise is often found as unrealistic pixel values at unexpected locations and is commonly referred to as the isolated pixel problem (IPP). Spectral classifiers do not entirely address the IPP as they refer only to the DN of image pixels for achieving image classification (Krishnapuram and Keller 1993). The suitable use of context allows the elimination of possible ambiguities, the recovery of missing information, and the correction of errors, thus improving the robustness of a spectral classifier against noise (Li 1995; Magnussen, Boudewyn, and Wulder 2004). By providing NC with additional information (e.g. information about the neighbourhood classes for a pixel), the classifier would more accurately predict the class to which a noisy point belongs.

In remote sensing, the energy reaching the sensor does not entirely correspond to the pixel area on the ground, as it also includes energy from neighbouring pixel areas. This is mostly caused by diffuse scattering of the incoming radiation due to atmospheric distortion. Moreover, classes on the ground usually span several pixels and it is rare to find a class in isolation. Hence, there exists a relation between a pixel and its neighbouring pixels. Markov random fields (MRFs) are used in effective modelling of such contextual relationships, in the case of context-dependent entities such as image pixels (Geman and Geman 1984; Li 2009). It has been widely used in image segmentation and image restoration (Derin and Elliott 1987; Dubes and Jain 1989; Tso and Olsen 2005). MRFs based upon simulated annealing optimization (Mather and Tso 2010) are widely accepted for modelling contextual information in images, since publication of the classical study by Geman and Geman (1984). This considerably improved the accuracy of PCM (Chawla 2010) and FCM (Singha et al. 2015) classifiers. In those studies, modelling of spatial contextual information was done using both the smoothness-prior MRF model (S-MRF) and four different discontinuity adaptive-MRF models (DA-MRF)(Li 2009). Among these models, the use of DA-MRF models has helped to produce a higher classification accuracy as compared with S-MRF models (Chawla 2010; Singha et al. 2015).

Accuracy assessment of a fuzzy classification is not straightforward, because multiple classes might be assigned to a single pixel and so the standard error matrix cannot be realized (Silván-Cárdenas and Wang 2008). Efforts to assess the accuracy of a fuzzy classification result after making it crisp resulted in loss of information (Foody 1997; Silván-Cárdenas and Wang 2008). Various suggestions have been provided to carry out a fuzzy image accuracy assessment (Binaghi et al. 1999; Congalton 1991; Green and Congalton 2004; Pontius and Cheuk 2006), but a standard accuracy assessment technique is still lacking. Among the various methods proposed, the fuzzy error matrix (FERM) has been widely accepted and hence was used in this study for accuracy assessment (Binaghi et al. 1999).

The aim of this paper is to present a novel hybrid fuzzy noise classifier, and then to study its effects on the classification accuracy. Here, the spatial contextual information was modelled using MRFs and thus incorporated into the fuzzy noise classifier, thus creating a novel hybrid classifier. This classifier was applied on advanced wide-field sensor (AWiFS) and linear imaging self-scanning Sensor-III (LISS-III) images from the

Resourcesat-1 satellite in Uttarakhand State in India. Results were evaluated with a linear imaging self-scanning Sensor-IV (LISS-IV) image.

## 2. Noise clustering

The presence of noise is often perceived as a problem for effective clustering, as it biases clustering algorithms and results in the formation of unrealistic clusters. Noise clustering is a fuzzy clustering technique which was developed to address this problem. It overcomes the possible problem of unrealistic cluster formation due to the presence of noise in the input image (Dave' 1993; Krishnapuram and Keller 1993) It achieves this immunity to noise by allocating noisy data into a separate class termed the noise class. The noise class cluster centre is selected such that it is equidistant from all points in the image, and thus each data point in the noise cluster has an equal prior probability of belonging to any other cluster. In noise clustering, data points beyond the noise distance ( $\delta$ ) from the cluster centres are considered as noise, but the pre-specification of  $\delta$  is not practical due to insufficient information about the data (Dave' 1991). In this study,  $\delta$  was estimated using the method mentioned in Section 3.2. Figure 1(a) shows sample data set taken from Dave' (1993) and Figure 1(b) shows the result of noise clustering on the image. Three valid clusters formed by noise clustering are represented in Figure 1(b) using unique symbols, whereas the '+' symbol represents the noisy data assigned to the noise class.

Mathematically, noise clustering is modelled as an optimization problem with Equation (1) as its objective function that needs to be minimized and Equation (2) as its constraint:

$$J_{NC}(U; V) = \sum_{i=1}^N \sum_{j=1}^C (u_{ij})^m d(\mathbf{x}_i, \mathbf{v}_j) + \sum_{i=1}^N (u_{i,C+1})^m \delta, \quad (1)$$

and

$$\sum_{j=1}^{C+1} u_{ij} \leq 1 \quad 1 \leq i \leq N. \quad (2)$$

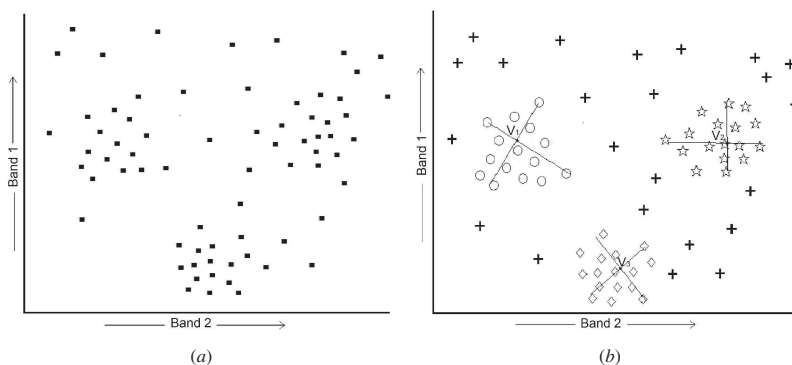


Figure 1. An example of cluster formation using noise clustering for  $C = 3$  classes and two spectral bands. (a) Noisy data and (b) clusters identified using noise clustering. In (b), '+' indicates the noise class.

In Equation (1),  $J_{NC}(U; V)$  corresponds to the value of the  $NC$  objective function for a particular  $U$  and  $V$ ,  $C$  is the number of classes,  $N$  is the total number of image pixels,  $m$  is the fuzzification factor,  $u_{ij}$  is the membership value of the  $i$ th pixel to the  $j$ th class, and  $u_{i,C+1}$  corresponds to the membership values of the noise class. Furthermore,  $\vec{v}_j$  denotes the vector pointing to the cluster centre of the  $j$ th class and  $\vec{x}_i$  is the membership value vector for the  $i$ th pixel. The Euclidian distance between  $\vec{x}_i$  and  $\vec{v}_j$  is represented by  $d(\vec{x}_i, \vec{v}_j)$ . Both  $\vec{x}_i$  and  $\vec{v}_j$  are vectors in a  $D$ -dimensional feature space, where  $D$  is the number of bands in the input image. The constraint  $\sum_{j=1}^{C+1} u_{ij} \leq 1$  allows the noisy data to achieve as low membership values as possible (Dave' and Krishnapuram 1997). The cluster centres are jointly represented by the set  $V = \{V_1, V_2, \dots, V_C\}$ , where  $V_1, V_2, \dots, V_C$  represent the cluster centres for the 1st, 2nd,  $\dots$ ,  $C$ th class. The set  $U = \{U_1, U_2, \dots, U_C, U_{C+1}\}$  contains the membership values for individual classes, where  $U_1, U_2, \dots, U_C$  represent the set of membership values for each pixel in the image and for each class, and  $U_{C+1}$  represents the set of membership values for each pixel in the image for the noise class. The value of the membership values  $u_{ij}$ , membership values for noise class  $u_{i,C+1}$ , and class mean vectors  $\vec{v}_j$  can be obtained from Equations (3), (4), and (5), respectively.

$$u_{ij} = \left[ \sum_{k=1}^C \left( \frac{d(\vec{x}_i, \vec{v}_j)}{d(\vec{x}_i, \vec{v}_k)} \right)^{\frac{1}{m-1}} + \left( \frac{d(\vec{x}_i, \vec{v}_j)}{\delta} \right)^{\frac{1}{m-1}} \right]^{-1} \quad (3)$$

$$u_{i,C+1} = \left[ \sum_{i=1}^C \left( \frac{\delta}{d(\vec{x}_i, \vec{v}_j)} \right)^{\frac{2}{m-1}} + 1 \right]^{-1} \quad (4)$$

$$\vec{v}_j = \frac{\sum_{i=1}^N ((u_{ij})^m (\vec{x}_i))}{\sum_{i=1}^N (u_{ij})^m} \quad (5)$$

In this article a supervised version of noise clustering, referred to as the fuzzy noise classifier (FNC), was used. The cluster centres  $V$  were initialized with the class mean vectors obtained from the supervised approach (i.e. for each class, random pixels were selected and pixel vectors were averaged to produce a mean vector). This also provides a computational advantage for the FNC as it reduces the number of iterations required to reach the optimal cluster centres, whereas it also ensures reproducibility of the results. More intuition on the need for cluster initialization can be obtained by understanding the objective function shown in Equation (1), which aims to minimize  $U$  and  $V$  simultaneously.

### 3. Methodology

The objective of this study was to develop an efficient hybrid classifier by integrating spatial contextual information onto the FNC, which uses only the spectral information to perform classification. To achieve this, an integral part of the methodology was to formulate the objective functions for (FNC)<sub>s</sub> and four (FNC)<sub>DA</sub> classifiers, where (FNC)<sub>s</sub> corresponds to the FNC with smoothness prior, (FNC)<sub>DA</sub> corresponds to FNC

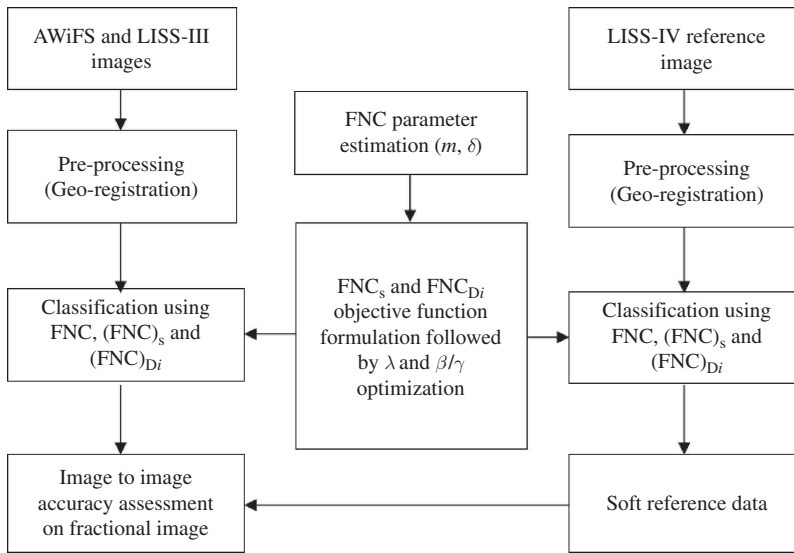


Figure 2. Methodology followed in this study. On the left side are the AWiFS and LISS-III images used to study the hybrid classifier performance, while on the right side is the LISS-IV image used for validation. All terms are defined in the text.

with discontinuity adaptive priors. Estimation of the parameters of the FNC and those of the hybrid classifier were carried out to ensure optimal performance. The accuracy assessment of the hybrid classifier, which is also a fuzzy classifier, was done using the FERM. Figure 2 shows the methodology used in this study.

Over-smoothing at the boundaries in an image, on using smoothness (S) MRF priors, was addressed in this study by replacing it with discontinuity adaptive (DA) MRF priors. These use an adaptive interaction function (AIF)  $h(\eta)$ , as a function of  $\eta$ , that is placed within the regularizer to model the nature of the interaction of a pixel site with its neighbours.  $\eta$  represents the difference in membership values between the centre pixel and its neighbour within a clique. A clique is a subset of a site from the neighbourhood system, where the members of the site are mutual neighbours (Mather and Tso 2010).  $h(\eta)$  returns a low value when the membership variation in the pixel neighbourhood is large, and returns a high value when the membership variation in the pixel neighbourhood is low, resulting in selective smoothing. Equation (6) shows the relation among AIF,  $h(\eta)$ , and the adaptive potential function (APF),  $g'(\eta)$ . The APF encodes the neighbourhood information for a pixel, and it is further incorporated into the objective function of the FNC to form the hybrid classifier.

$$g'(\eta) = 2\eta h(\eta) \quad (6)$$

Four AIFs from the literature are used in this work (Equations (7)–(10)), resulting in four different APFs and hence four different DA models (Li 2009). Each AIF has a unique response graph, and in this way models the interaction between a pixel site and its neighbours in a different way. In Equations (7)–(10), the parameter  $\gamma$  controls the intensity of the interaction between a pixel and its neighbours. Incorporation of each of these APFs

into the objective function of FNC created a new hybrid classifier, and are referred to in this study as (DA)<sub>1</sub>, (DA)<sub>2</sub>, (DA)<sub>3</sub>, and (DA)<sub>4</sub> MRF models, respectively.

$$h_1(\eta) = \exp\left(\frac{-\eta^2}{\gamma}\right) \tag{7}$$

$$h_2(\eta) = \frac{1}{\left[\frac{1}{1+\frac{\eta^2}{\gamma}}\right]^2} \tag{8}$$

$$h_3(\eta) = \frac{1}{1 + \frac{\eta^2}{\gamma}} \tag{9}$$

$$h_4(\eta) = \frac{1}{1 + \frac{|\eta|}{\gamma}} \tag{10}$$

**3.1. Mathematical formulation of hybrid classifiers**

The FNC achieves classification by solving an optimization problem, as stated in Equations (1) and (2). The hybrid classifiers were created by adding a spatial term to the objective function of the FNC while keeping its optimization problem constraint unchanged. Spatial contextual information was modelled using all four different DA-MRF models mentioned in Section 3, separately. Modelling was also done using the S-MRF model for showing the performance improvement of the classifier against the four DA-MRF models. Using Bayes theorem we were able to incorporate the spatial information modelled using MRFs into Equation (1), hence formulating the objective function for the hybrid classifier.

The formulated objective function of the (FNC)<sub>S</sub> classifier is shown in Equation (11):

$$E(u_{ij}) = (1 - \lambda) \left[ \sum_{i=1}^N \sum_{j=1}^C (u_{ij})^m d(\vec{x}_i, \vec{v}_j) + \sum_{i=1}^N (u_{i,C+1})^m \delta \right] + \lambda \left[ \sum_{i=1}^N \sum_{j=1}^C \sum_{j \in N_j} \beta(u_{ij} - u_{ij'})^2 \right]. \tag{11}$$

The term *E* in Equation (11) refers to the energy of the pixel for the membership value *u<sub>ij</sub>*. The remainder of the terms in Equation (11) are defined in Section 2. The optimization of Equation (11) is done using simulated annealing (Mather and Tso 2010). Objective functions of the (FNC)<sub>D<sub>i</sub></sub> classifiers for *i* = 1, . . . , 4 are formed by replacing the APF (i.e. the term  $\beta(u_{ij} - u_{ij'})^2$  in Equation (11)), with the corresponding APFs being equal to  $-\gamma \exp\left(\frac{-\eta^2}{\gamma}\right)$ ,  $\frac{-\gamma}{\left[\frac{1}{1+\frac{\eta^2}{\gamma}}\right]^2}$ ,  $\gamma \ln\left(1 + \frac{\eta^2}{\gamma}\right)$ , and  $\gamma|\eta| - \gamma^2 \ln\left(1 + \frac{|\eta|}{\gamma}\right)$ , respectively (Li 2009). In

this way, (FNC)<sub>S</sub> and the (FNC)<sub>D<sub>i</sub></sub> represent the hybrid classifiers obtained by using the *S* and (DA)<sub>*i*</sub> MRF models for *i* = 1, . . . , 4, respectively.

The term  $\lambda$  is used in the objective function of the hybrid classifier to balance the contribution of information from the spectral and spatial domains. This further controls

the impact of spatial and spectral information on the classification. The weights  $\beta$  control the amount of influence of a site with its neighbours.

### 3.2. Fuzzy noise classifier parameter estimation

The outputs of FNC are fractional images, where each pixel depicts the membership values (i.e. the possibilistic percentage cover of a particular class within that pixel). The classifier generates a fractional image for each individual class.

Estimation of the FNC parameter, which includes the noise distance ( $\delta$ ) and the fuzzification factor ( $m$ ), is essential for ensuring the best performance of the FNC. The parameter combination which gives the maximum classification accuracy for the FNC was considered. Accuracy of the fuzzy classification was assessed by minimizing the entropy associated with the fractional images (Dehghan and Ghassemian 2006). Entropy minimization is a widely accepted method to quantify the uncertainty associated with an image. To calculate the entropy of a class, random pixels were selected from the high-membership regions of the fractional image for each class. Vectors of membership values were formed for each pixel by combining membership values from all the fractional images. For each such membership vector, the entropy was calculated using Equation (12) and was averaged to obtain the entropy for a pixel.

$$H_{\text{avg}} = \frac{\sum_{i=1}^C (u_{ij}) \log_2(u_{ij})}{\sum_{i=1}^C (u_{ij})} \quad (12)$$

Entropy as the sole criterion for optimal parameter estimation was found to be insufficient, as the minimum entropy fractional images could possibly be generated from a parameter combination, resulting in inaccurate classification. To address this problem, accuracy estimation was done using inter-class membership change calculation (IMC), which is based on the fact that, in the optimal classification, the membership value of class pixels will be highest in the fractional image associated with that class only, but corresponding pixel membership values will be lowest in the other fractional images (Townsend 2000). In this method, emphasis is given to finding parameters that maximize this difference in membership values for all class pixels. To do so, the difference is calculated for a fractional image between the mean membership values at known class locations, and the mean of membership values at known non-class locations. A large difference corresponds to a more accurate classification. The FNC estimates were found by simultaneously minimizing the entropy of the fractional image and maximizing the IMC.

### 3.3. Hybrid classifier parameter estimation

The hybrid classifier was developed by adding a spatial term to the FNC formulation. For the hybrid classifier, two parameters need to be estimated. The first is the weight factor  $\lambda$ , with  $0 \leq \lambda \leq 1$ , which controls the impact of spatial and spectral components. The second is  $\beta$  in the case of S-MRF, or  $\gamma$  in case of a DA-MRF. Both parameters have an impact on the classification accuracy, and hence their estimation is critical.

The main objective behind the use of DA models is to preserve the class boundaries during classification, considered as the main criterion for hybrid parameter estimation. To



determine the optimal parameter values, the classification was repeated with different combinations of  $\lambda$  and  $\beta$  in the case of S-MRF and  $\lambda$  and  $\gamma$  in the case of DA-MRF. The range of  $\beta$  was set to [1, 10] and that of  $\gamma$  to [0, 1], as values outside this range were found to significantly reduce the overall classification accuracy.

Edge preservation in the fractional images was quantified in this study using the mean-variance method (Chawla 2010; Singha et al. 2015). This method considers the mean difference in membership values across boundaries, as well as the membership variance on either side of boundaries, as a means to quantify the edge preservation in the fractional images. Fractional images with the highest mean difference in membership values across boundaries and minimum membership value variance on either side of the boundaries provided the best results in terms of edge preservation. Ultimately the parameter combination which provided the highest edge preservation in the classification results was considered as the hybrid classifier parameter estimates.

Once the FNC and hybrid classifier parameters were estimated, the optimal membership values, and hence the fractional images, were found by minimizing Equation (11) using simulated annealing (SA) optimization (Mather and Tso 2010; Geman and Geman 1984). When using SA, the initial temperature ( $T_0$ ) was set to 3 and the temperature update rate ( $k$ ) was set to 0.90 for efficient optimization. These values were considered because the variance in the estimates was minimal on repeating the estimation (Tolpekin and Stein 2009).

### 3.4. Accuracy assessment

To quantify the accuracy of fuzzy classifiers, the error matrix that is commonly applied for hard classification cannot be used. In this study we used the FERM (Zhang and Foody 1998). This is similar to the error matrix, but it takes fractional images as its input. Hence the cell values are between 0 and 1. This is based on the min operator (intersection operator), which shows the maximum possible overlap between reference and classified image and is calculated as shown in Equation (13) (Silván-Cárdenas and Wang 2008). In Equation (13),  $P_{nij}$  is the maximum possible overlap between the reference and the classified image,  $u_{ij}$  and  $v_{ij}$  represent membership values of the  $i$ th pixel in the fractional image for class  $j$  in the assessed and reference image, respectively.

$$P_{nij} = \min(u_{ij}, v_{ij}) \quad (13)$$

The efficiency of the novel hybrid classifier was obtained by evaluating its performance on coarse-resolution (56 m) AWiFS and medium-resolution (23.5 m) LISS-III images. Fractional images generated from high-resolution (5.6 m) LISS-IV image values were used as the reference image. For accuracy assessment, the cell resolutions of AWiFS, LISS-III, and LISS-IV images were resampled so that their resolutions were in the ratio 1:4:12. Hence 16 pixels ( $4 \times 4$ ) of LISS-III and 144 pixels ( $12 \times 12$ ) of AWiFS were combined (pixel values averaged) to achieve the pixel dimension of the LISS-IV image. In this way, an effective comparison could be made between images of different resolutions. Resampling of the images and aggregation of pixel values were potential sources of error, but were ignored in this study since they were likely to be very small. We applied nearest neighbour resampling, resulting in geometric discontinuities in the order of plus or minus half the pixel size, which is considered acceptable (Chawla 2010).

#### 4. Study area and data

The study area is the Sitarganj Tehsil, Udham Singh Nagar District, Uttarakhand State, India, located at 28° 52' 29" N to 28° 54' 20" N and 79° 34' 25" E to 79° 36' 34" E. Uttarakhand is a state in the northern part of India and Sitarganj Tehsil is located in the southern part of the state. Sitarganj Tehsil is near Pand Nagar Agricultural University, famous for its participation in the Green Revolution of India. The study area was selected for its diversity in classes. The current research aims at testing the capability of a novel classifier, and Sitarganj Tehsil has a large diversity of distinguishable classes. Six classes were identified from the study area and are labelled in Figure 3. The study area mostly includes sugarcane and paddy agricultural farms. It also has two large reservoirs, named Dhora and Bhagul, on the northwestern and southeastern parts, respectively. Images from AWiFS and LISS-III sensors on board Resourcesat-1 were used to study the efficiency of the novel hybrid classifier considered in this work. The AWiFS (56 m), LISS-III (23.5 m), and LISS-IV (5.8 m) images were acquired on the same date (15 October 2007), and hence are comparable. The validation of classification was done against the LISS-IV image of the same area. In this study, the LISS-IV image was rectified using Survey of India (SOI) toposheet no. 53P/9. Geo-registration of the AWiFS and LISS-III images was conducted using the geometrically corrected LISS-IV image. Figure 3 shows the high-resolution LISS-IV image of the study area. The AWiFS and LISS-III images provide the low- and medium-resolution images of the same area.

Ground data validation was not preferred in this study, as it is difficult to identify a pixel area on the ground. Also it is impractical to manually quantify the percentage cover

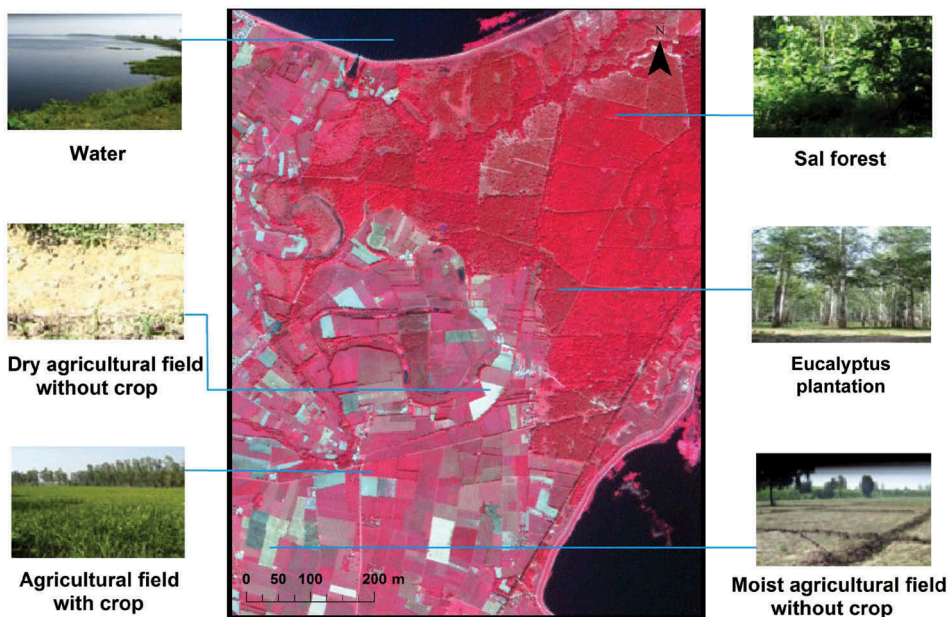


Figure 3. LISS-4 imagery (from Resourcesat-1) of Sitarganj Tehsil, Udham Singh Nagar District, Uttarakhand, India, acquired on 15 October 2007. The image is a false color composite (FCC) image with 0.77–0.86  $\mu\text{m}$  spectral band mapped to the Red band, an FCC image with 0.62–0.68  $\mu\text{m}$  spectral band mapped to the Green band, and a 0.52–0.59  $\mu\text{m}$  spectral band mapped to the Blue band.

of a particular class within an area on the ground, as the certainty with which the classes can be identified is a subjective issue (Foody 2000).

## 5. Results

### 5.1. Fuzzy noise classifier parameter estimates

Parameters for both the FNC and the hybrid classifier were estimated separately for each image considered in this study. On analysing the FNC results for different parameter values,  $\delta$  was found to have minimal or no impact on the value of total entropy or IMC beyond the threshold  $\delta = 10,000$ . For  $\delta < 100$ , unrealistic classification emerged and so these values were omitted. Figure 4 shows the effect of  $\delta > 100$  on  $m$  for the ‘Agricultural Field with Crop’ class in the AWiFS image. As can be observed, estimated  $m$  values are least affected by changes in  $\delta$  beyond  $\delta = 10,000$ . So  $m$  was estimated while maintaining  $\delta = 10,000$ . Estimation was done separately for each fractional image (or class) generated by FNC.

The FNC parameters were estimated using the normalized entropy graph and the IMC graph, as shown in Figure 5. In particular, the entropy versus IMC graph of the AWiFS

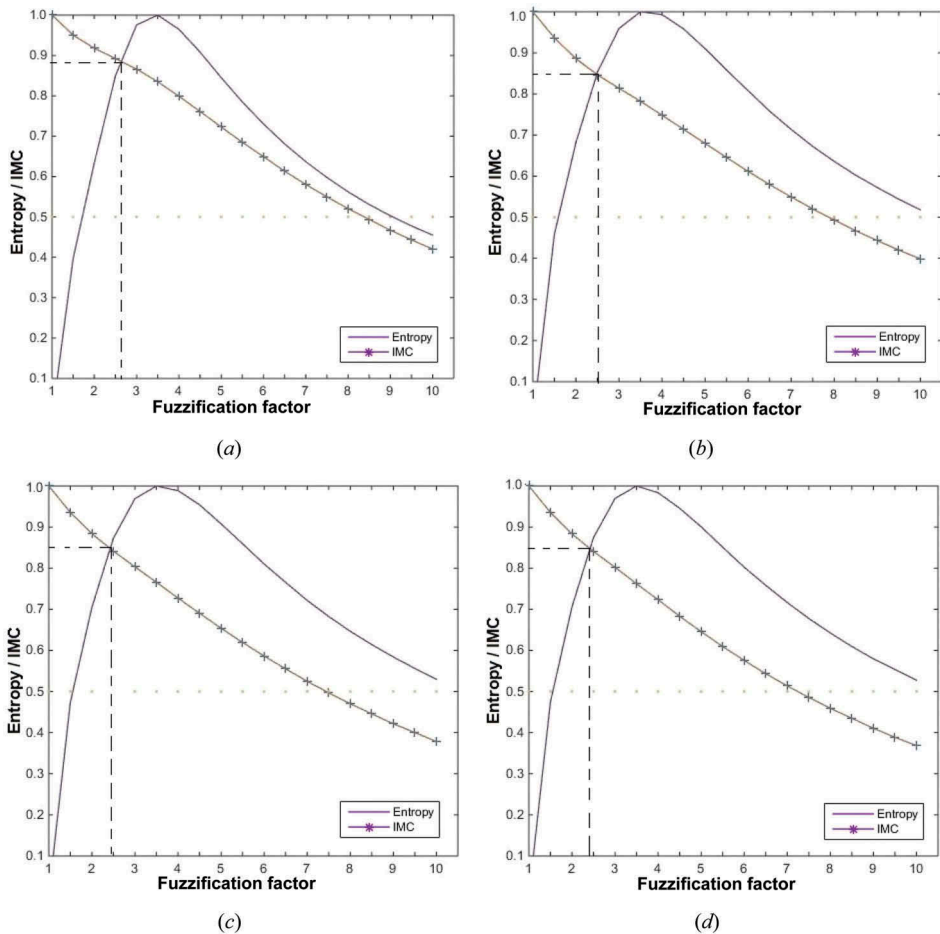


Figure 4. Effect of  $\delta$  on estimation of  $m$  for the ‘Agricultural Field with Crop’ class in the AWiFS image, for different values of  $\delta$ : (a)  $\delta = 100$ , (b)  $\delta = 1000$ , (c)  $\delta = 10,000$ , and (d)  $\delta = 50,000$ .

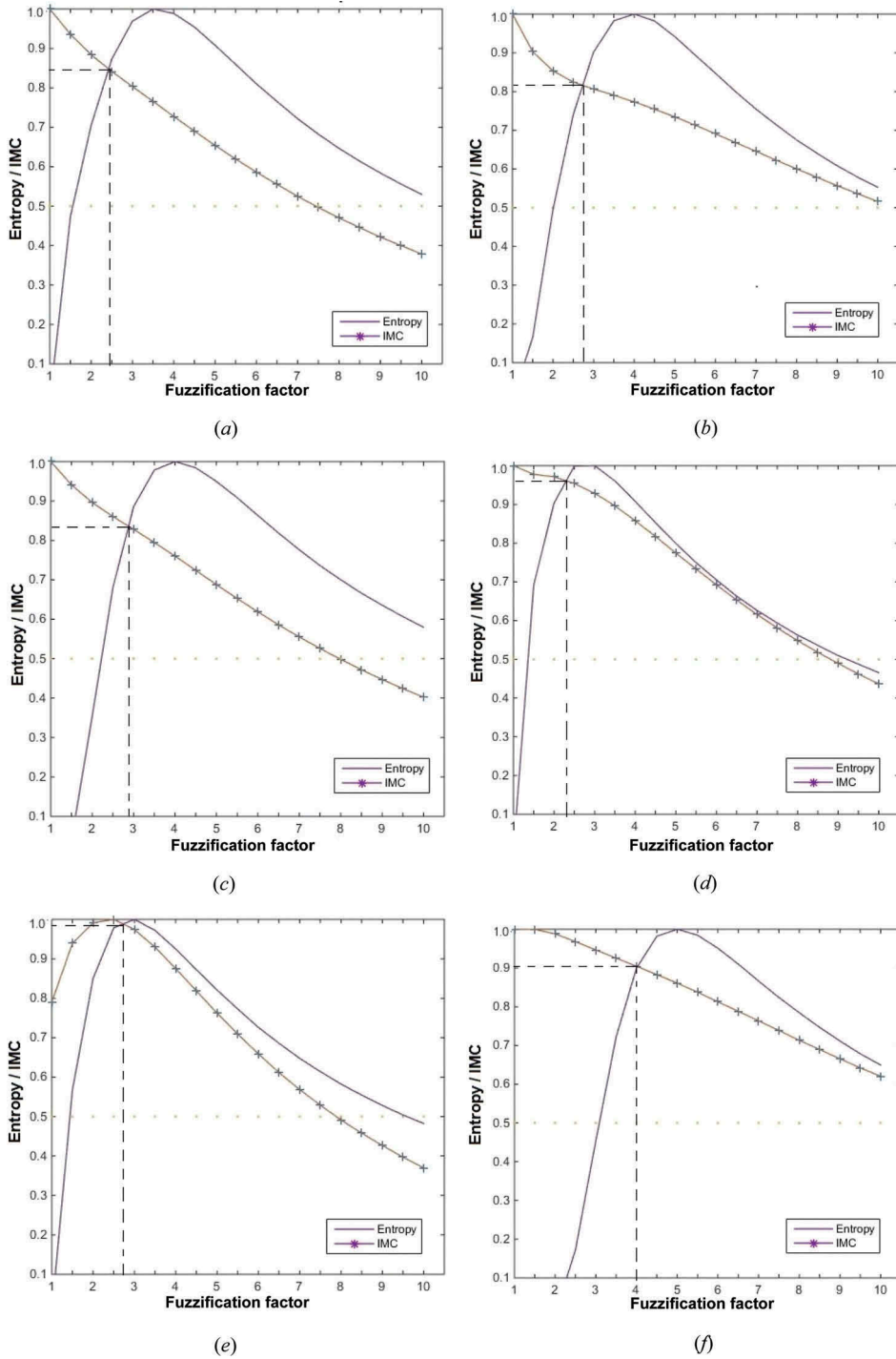


Figure 5. Entropy/IMC versus fuzzification factor plots for different LULC classes considered in the AWiFS image. (a) Agricultural field with crop, (b) Sal forest, (c) Eucalyptus plantation, (d) Dry agricultural field without crop, (e) Moist agricultural field without crop, and (f) Water.

Table 1. Fuzzification factor  $m$  estimates obtained against the low-, medium-, and high-spatial resolution (reference) images for the FNC.

| Image    | Fuzzification factor ( $m$ ) |
|----------|------------------------------|
| AWiFS    | 2.7                          |
| LISS-III | 2.9                          |

image is shown in Figure 5. Mean  $m$  estimates, obtained for AWiFS and LISS-III images, are shown in Table 1. Optimal  $m$  value estimation for the reference image (i.e. LISS-IV) was also essential to obtain the best possible soft reference data. For the LISS-IV image, the optimal  $m$  value was found to be 3.0. Visual inspection of the optimal fractional images generated using the estimated parameter values showed them to be very accurate, and this added to confidence in the estimates.

From Table 1, it will be seen that  $m$  shows a slightly increasing trend with increase in the spatial resolution of the images, which in turn is caused by the increase in entropy of an image with an increase in its resolution. This is just an observation which was made and has no impact on the results of this study.

## 5.2. Hybrid classifier parameter estimates

Parameter estimates for the hybrid classifier were obtained against the fractional images quantified as having maximum edge preservation. Quantification of edge preservation in the fractional images was conducted using the mean-variance method as explained in Section 3.3. Estimates for the hybrid classifier obtained for the low-spatial resolution AWiFS and medium-spatial resolution LISS-III images, for different MRF models, are shown in Table 2.

As was the case with FNC parameter estimation, the hybrid parameters were estimated for the high-spatial resolution reference image (i.e. LISS-IV) to generate the optimal soft reference data. The hybrid parameter estimates for the LISS-IV image are shown in Table 3.

Among the different DA-MRF prior models used in this study, a combination of the  $(DA)_4$  model with the FNC (i.e. the  $(FNC)_{D4}$  classifier) showed the maximum edge preservation capability. This was observed for all three images considered in this study. Figures 6 and 7 show the fractional images generated by FNC for AWiFS and LISS-III images, respectively, whereas fractional images generated by the  $(FNC)_{D4}$  classifier for the AWiFS and LISS-III images are shown in Figures 8 and 9, respectively. In the case of the

Table 2. Hybrid classifier estimates obtained against the low- and medium-spatial resolution images.

| Hybrid Classifier | MRF Model | AWiFS     |                | LISS-III  |                |
|-------------------|-----------|-----------|----------------|-----------|----------------|
|                   |           | $\lambda$ | $\beta/\gamma$ | $\lambda$ | $\beta/\gamma$ |
| $(FNC)_S$         | S         | 0.6       | 5.0            | 0.9       | 5.0            |
| $(FNC)_{D1}$      | $(DA)_1$  | 0.9       | 0.4            | 0.9       | 0.5            |
| $(FNC)_{D2}$      | $(DA)_2$  | 0.7       | 0.8            | 0.8       | 0.4            |
| $(FNC)_{D3}$      | $(DA)_3$  | 0.7       | 0.9            | 0.8       | 0.5            |
| $(FNC)_{D4}$      | $(DA)_4$  | 0.8       | 0.8            | 0.9       | 0.7            |

Table 3. Hybrid classifier estimates obtained against the high-spatial resolution reference images.

| Hybrid Classifier | MRF Model       | LISS-IV   |                |
|-------------------|-----------------|-----------|----------------|
|                   |                 | $\lambda$ | $\beta/\gamma$ |
| $(FNC)_S$         | S               | 0.6       | 6.0            |
| $(FNC)_{D1}$      | DA <sub>1</sub> | 0.9       | 0.4            |
| $(FNC)_{D2}$      | DA <sub>2</sub> | 0.7       | 0.5            |
| $(FNC)_{D3}$      | DA <sub>3</sub> | 0.7       | 0.7            |
| $(FNC)_{D4}$      | DA <sub>4</sub> | 0.8       | 0.5            |

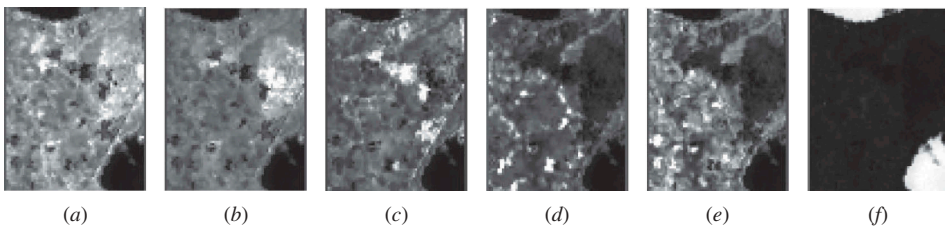


Figure 6. Fractional images obtained against AWiFS image for the FNC for (a) Agricultural fields with crops, (b) Sal forest, (c) Eucalyptus plantations, (d) Dry agricultural fields without crops, (e) Moist agricultural fields without crops, and (f) Water.

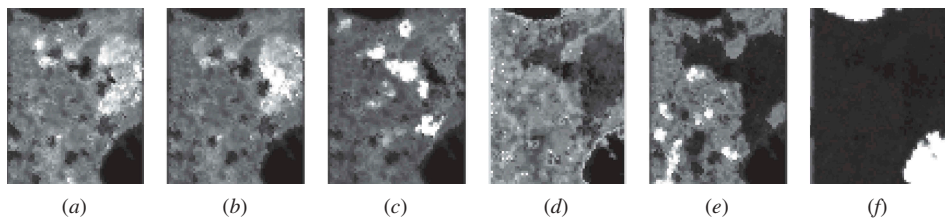


Figure 7. Fractional images obtained against the LISS-III image for the FNC for (a) Agricultural fields with crops, (b) Sal forest, (c) Eucalyptus plantation, (d) Dry agricultural fields without crops, (e) Moist agricultural fields without crops, and (f) Water.

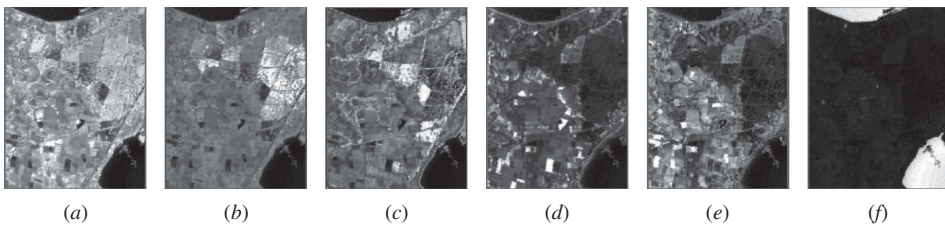


Figure 8. Fractional images obtained against AWiFS image for the  $(FNC)_{D4}$  classifier, (a) for Agricultural fields with crop, (b) Sal Forest, (c) Eucalyptus plantation, (d) Dry agricultural field without crop, (e) Moist agricultural field without crop, and (f) Water.

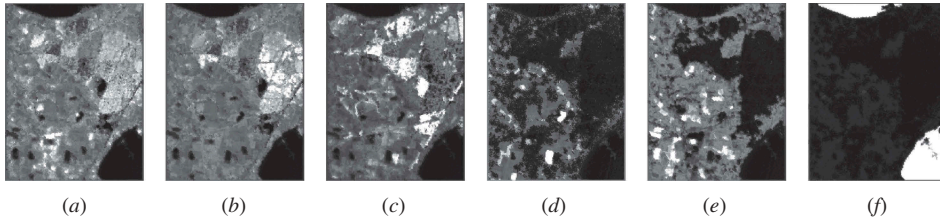


Figure 9. Fractional images obtained against the LISS-III image for the  $(FNC)_{D4}$  classifier for (a) Agricultural fields with crops, (b) Sal forest, (c) Eucalyptus plantation, (d) Dry agricultural fields without crops, (e) Moist agricultural fields without crops, and (f) Water.

$(FNC)_{D4}$  classifier, the membership values of unrealistic isolated pixels were reduced thus achieving a more realistic classification. The  $(FNC)_{D4}$  classifier achieves this by selective smoothing of pixels as explained in Section 3. Also, a reduction in the accuracy is observed for fractional images produced for the AWiFS image when compared with those of the LISS-III image, caused by the lower resolution of AWiFS as compared with LISS-III.

### 5.3. Accuracy assessment results

Table 4 shows the FERM overall fuzzy accuracy of classification results for AWiFS against LISS-IV reference images and LISS-III against LISS-IV reference images for FNC,  $(FNC)_S$ ,  $(FNC)_{D1}$ ,  $(FNC)_{D2}$ ,  $(FNC)_{D3}$ , and  $(FNC)_{D4}$  classifiers.

justification = centring

Among the different classifiers formed,  $(FNC)_{D4}$  gave the highest overall fuzzy accuracy, of 87.3% for AWiFS and 89.4% for LISS-III images. The APF functions are usually convex, and there exists a region of  $\eta$  within which the smoothing strength therefore increases monotonically with increase in  $|\eta|$ . A perfectly convex APF function will result in no smoothing at the boundaries, and the smoothing strength gradually increases on moving away from the boundaries. This type of smoothing blends well with the concept of gradual class variation at the boundaries in natural objects. The APF of  $(DA)_4$  is a smoother convex function than those of its counterparts (Li 2009) and therefore performs better. It will be observed that the use of  $S$ ,  $(DA)_2$ , and  $(DA)_3$  MRF

Table 4. FERM overall fuzzy accuracy obtained on comparing the low- and medium-spatial resolution fractional images with the high-resolution reference fractional image, for the trained case.

| Classifier   | Accuracy (%)         |                         |
|--------------|----------------------|-------------------------|
|              | AWiFS versus LISS-IV | LISS-III versus LISS-IV |
| FNC          | 83.2                 | 87.3                    |
| $(FNC)_S$    | 82.7                 | 88.2                    |
| $(FNC)_{D1}$ | 84.6                 | 87.6                    |
| $(FNC)_{D2}$ | 81.8                 | 77.0                    |
| $(FNC)_{D3}$ | 81.4                 | 75.6                    |
| $(FNC)_{D4}$ | 87.3                 | 89.4                    |

models for spatial contextual modelling resulted in a slight reduction in the accuracy of the FNC for all the images considered in this study. Also, while acquiring higher-spatial resolution data by a sensor, intra-pixel neighbour-reflectance effect resulted due to a single class, whereas in coarser spatial images this effect is due to an increased number of classes. This neighbour effect is added as noise to a pixel, and hence the coarser pixels have a stronger neighbour pixel effect than high-resolution pixels. For the same reason,  $(DA)_4$  produces greater improvement in accuracy for the AWiFS image than for the LISS-III image.

#### 5.4. Performance with untrained classes

The FNC considers any class other than those of interest as image noise. To quantify the robustness of FNC to noise, a class was deliberately omitted while training the classifier and the performance of the classifier was then evaluated (i.e., the classifier was deprived of the signature information about one known class and classification was done). The results obtained for one such experiment are shown in Table 5.

Here the class ‘Agricultural Fields with Crops’ was left untrained for both AWiFS and LISS-III images. Table 5 compares the user’s accuracy of FNC,  $(FNC)_S$ , and  $(FNC)_{D4}$  classification results for AWiFS and LISS-III images for both the trained and untrained case, using the  $(FNC)_{D4}$  classifier. The other hybrid classifiers were not considered for this analysis, as they are of relatively low accuracy when compared with the  $(FNC)_{D4}$  classifier. It can be seen from Table 5 that the user’s accuracy obtained in the presence of an untrained class was low when compared with user’s accuracy if all classes are trained. For the AWiFS data, the decrease in user’s accuracy in the untrained case was 9.2%, 10.1%, and 9.9% for FNC,  $(FNC)_S$ , and  $(FNC)_{D4}$ , respectively. For the LISS-III data, the decrease in user’s accuracy for the untrained case was 11.0%, 12.2%, and 6.0% for FNC,  $(FNC)_S$  and  $(FNC)_{D4}$  respectively. The decrease in user’s accuracy for the untrained case is due to the increased number of untrained classes, which are added to the pixel as noise. Even though the FNC clearly has the ability to restrict the information flow from untrained classes in an image, the results from Table 5 show that the performance of FNC classifiers decreases when there is an increase in noise. The relatively small drop in user’s accuracy for AWiFS as compared with LISS-III can be explained by the intra-pixel neighbourhood reflectance effect, as explained in Section 5.3.

Table 5. Fuzzy user’s accuracy obtained for the trained and untrained cases, for low- and medium-spatial resolution images.

| Classifier   | Accuracy (%)         |         |                         |         |
|--------------|----------------------|---------|-------------------------|---------|
|              | AWiFS versus LISS-IV |         | LISS-III versus LISS-IV |         |
|              | Untrained            | Trained | Untrained               | Trained |
| FNC          | 74.8                 | 84.0    | 77.2                    | 88.2    |
| $(FNC)_S$    | 75.6                 | 85.7    | 76.3                    | 88.5    |
| $(FNC)_{D4}$ | 55.0                 | 64.9    | 69.4                    | 75.4    |



### 5.5. Comparison with results of previous studies

In various studies, information from the spectral, spatial, and temporal domains has been used, in all possible permutations, to achieve better image classification. Among these, the studies conducted for evaluating the impact of incorporating spatial contextual information, modelled using MRF in combination with FCM (Singha et al. 2015), and with possibilistic c-means classification (Chawla 2010), are closely related to ours. Also, they have all used the same data sets that were used for this study.

The results of these studies were compared with those of the FNC-MRF classifier. In the case of FCM,  $(DA)_3$ -MRF prior gave the best results and the overall fuzzy accuracy for AWiFS and LISS-III images was 85.5% and 89.5%, respectively (Singha et al. 2015). In the case of PCM,  $(DA)_2$ -MRF prior proved to be the best and its overall fuzzy accuracy for AWiFS and LISS-III images was 82.0% and 87.3%, respectively (Chawla 2010). Upon comparing the overall fuzzy accuracy of  $(FNC)_{D4}$  with  $(FCM)_{D3}$ , one can see that there is an improvement in accuracy of 1.8% for the AWiFS image for  $(FNC)_{D4}$  and almost the same for LISS-III image. When comparing the overall fuzzy accuracy of  $(FNC)_{D4}$  to  $(PCM)_{D2}$ , one can see that there is an improvement in accuracy of 5.3% and 2.1% for  $(FNC)_{D4}$  against AWiFS and LISS-III images, respectively. This proves the ability of the FNC to produce better classification results when supported by spatial contextual information.

## 6. Discussion

The hybrid classifiers developed in this study combine the DN value of a pixel from the spectral domain with the context of the pixel in the spatial domain. The spatial contextual information for a pixel was modelled using four different discontinuity adaptive MRF models, and the impact of adding information to the FNC was studied. Mathematically, the FNC is expressed as an optimization function and hybrid classifiers were created by adding the APFs of the MRF models as additional terms in the objective function. The weight factor,  $\lambda$  allowed control of the contribution from the spatial and spectral terms of the hybrid classifier. For  $\lambda = 0$ , the spatial context of a pixel does not affect the classification, whereas for  $\lambda = 1$ , classification will be performed based on the spatial context of a pixel. The optimal value of  $\lambda$  was found to be dependent on the resolution of the image and was estimated using the methods in Section 3.3.

The MRF helps in achieving better classification by smoothing the unrealistic pixel locations in an image, thus addressing the isolated pixel problem. The DA-MRF model ensures that smoothing happens only within a class and not at the class boundaries. As a result, the final fractional images produced by the hybrid classifier appear more like a smoothed version of the original FNC outputs, resulting in a small decrease in the classification accuracy. However, the increase in accuracy obtained by reducing the isolated pixel problem and the mixed pixel problem outweighs this decrease due to increased smoothness. Each MRF has a unique AIF, and as a result their effectiveness in spatial contextual modelling is different even for the same image. Since no method exists to predict the potential of using an MRF model for an image, spatial modelling was done using all five MRF models to compare their performance and thus identify the best model. The parameters associated with these models, such as  $\beta$  and  $\gamma$ , were also found to be data dependent and to have an impact on the classification accuracy. The hybrid classifier parameter estimates were the values that produced the highest edge preservation in the classification result.

FNC clearly has the ability to restrict the information flow from untrained (non-interested) classes in an image. For each hybrid classifier considered in this study, the presence of untrained classes in the input image caused a decrease in the classification accuracy. This is because the untrained classes are added to the pixel as noise. Nevertheless, there is an 14.1% improvement in the classification accuracy of  $(FNC)_{D4}$  as compared with classification by the  $(FCM)_{D3}$  classifier for the LISS-III image (Singha et al. 2015). This clearly shows the robustness of the  $(FNC)_{D4}$  classifier to the presence of untrained classes in the image as compared with the PCM- or FCM-based hybrid classifier. Hence the  $(FNC)_{D4}$  classifier should be selected in case there are untrained classes or unrealistic isolated pixels in the input image.

The current study was conducted on low-resolution (AWiFS) and medium-resolution (LISS-III) images only. Within the scope of the images used in this study, it was found that the  $(FNC)_{D4}$  classifier, which uses the  $(DA)_4$  MRF model, is the best. This is because the APF of  $(DA)_4$  is a smoother convex function with no smoothing at the boundaries and the smoothing strength gradually decreases on moving away from the boundaries. This type of smoothing blends well with the concept of gradual class variation at the boundaries in nature. The fuzzy nature of the FNC enabled the hybrid classifier to address the mixed pixel problem, whereas the use of spatial contextual information helped in addressing the isolated pixel problem, thus making the  $(FNC)_{D4}$  more efficient than the FNC. Nevertheless, to confirm the general usability of this classifier in remote-sensing studies, its classification accuracy must also be evaluated for images of other resolution with different set of classes, this is left to future studies.

## 7. Conclusion

The article studied the effect of adding spatial contextual information to a spectral classifier. A supervised version of noise clustering was used in this study, as the spectral classifier. Modelling of the spatial contextual information at the pixel level was achieved using the MRF technique. Both coarse- (AWiFS) and medium-resolution (LISS-III) images from Resourcesat-1 were used for evaluating the performance of the novel hybrid  $(FNC)_{DA}$  classifier. Among the different discontinuity adaptive MRF models used, the  $(FNC)_{D4}$  classifier was found to provide the highest classification accuracy for both images. The overall FERM accuracy for the  $(FNC)_{D4}$  classifier was found to be 87.3% and 89.4%, respectively, for the AWiFS and LISS-III images. Classification was also conducted by keeping a class untrained, to study the effects on  $(FNC)_{DA}$  accuracy of undesirable classes present in an image. In that case, a decrease in user's accuracy of 9.9% and 6.0% was observed for AWiFS and LISS-III, respectively, as compared with the fully trained case. The study concludes that the use of spatial contextual information improved the classification accuracy of the fuzzy noise classifier (FNC) when compared with the accuracy obtained on using FCM or PCM.

## Disclosure statement

No potential conflict of interest was reported by the authors.

## References

- Bezdek, J. C., R. Ehrlich, and W. Full. 1984. "FCM: The Fuzzy C-Means Clustering Algorithm." *Computers & Geosciences* 10 (2): 191–203. doi:[10.1016/0098-3004\(84\)90020-7](https://doi.org/10.1016/0098-3004(84)90020-7).

- Binaghi, E., P. A. Brivio, P. Ghezzi, and A. Rampini. 1999. "A Fuzzy Set-Based Accuracy Assessment of Soft Classification." *Pattern Recognition Letters* 20 (9): 935–948. doi:10.1016/S0167-8655(99)00061-6.
- Chawla, S. 2010. *Possibilistic C-Means-Spatial Contextual Information Based Sub-Pixel Classification Approach for Multi-Spectral Data*. Enschede: University of Twente, Faculty of Geo-Information and Earth Observation (ITC).
- Congalton, R. G. 1991. "A Review of Assessing the Accuracy of Classifications of Remotely Sensed Data." *Remote Sensing of Environment* 37 (1): 35–46. doi:10.1016/0034-4257(91)90048-B.
- Dave', R. N. 1991. "Characterization and Detection of Noise in Clustering." *Pattern Recognition Letters* 12: 657–664. doi:10.1016/0167-8655(91)90002-4.
- Dave', R. N. 1993. "Robust Fuzzy Clustering Algorithms." In *Second IEEE International Conference on Fuzzy Systems*, San Francisco, CA, March 28, 1993–April 01, 1993, vol 2, 1281–1286.
- Dave', R. N., and R. Krishnapuram. 1997. "Robust Clustering Methods: A Unified View." *IEEE Transactions on Fuzzy Systems* 5 (2): 270–293. doi:10.1109/91.580801.
- Dehghan, H., and H. Ghassemian. 2006. "Measurement of Uncertainty by the Entropy: Application to the Classification of MSS Data." *International Journal of Remote Sensing* 27 (18): 4005–4014. doi:10.1080/01431160600647225.
- Derin, H., and H. Elliott. 1987. "Modeling and Segmentation of Noisy and Textured Images Using Gibbs Random Fields." *IEEE Transactions on Pattern Analysis and Machine Intelligence* 9 (1): 39–55. doi:10.1109/TPAMI.1987.4767871.
- Dubes, R. C., and A. K. Jain. 1989. "Random Field Models in Image Analysis." *Journal of Applied Statistics* 16 (2): 131–164. doi:10.1080/02664768900000014.
- Foody, G. M. 1997. "Fully Fuzzy Supervised Classification of Land Cover from Remotely Sensed Imagery with an Artificial Neural Network." *Neural Computing & Applications* 5 (4): 238–247. doi:10.1007/BF01424229.
- Foody, G. M. 2000. "Estimation of Sub-Pixel Land Cover Composition in the Presence of Untrained Classes." *Computers & Geosciences* 26 (4): 469–478. doi:10.1016/S0098-3004(99)00125-9.
- Geman, S., and D. Geman. 1984. "Stochastic Relaxation, Gibbs Distributions, and the Bayesian Restoration of Images." *IEEE Transactions on Pattern Analysis and Machine Intelligence* 6 (6): 721–741. doi:10.1109/TPAMI.1984.4767596.
- Green, K., and R. G. Congalton. 2004. *An Error Matrix Approach to Fuzzy Accuracy Assessment: The NIMA Geocover Project*. Boca Raton, FL: CRC Press. eBook ISBN : 978-0-203-49758-6.
- Krishnapuram, R., and J. M. Keller. 1993. "A Possibilistic Approach to Clustering." *IEEE Transactions on Fuzzy Systems* 1 (2): 98–110. doi:10.1109/91.227387.
- Krishnapuram, R., and J. M. Keller. 1996. "The Possibilistic C-Means Algorithm: Insights and Recommendations." *IEEE Transactions on Fuzzy Systems* 4 (3): 385–393. doi:10.1109/91.531779.
- Li, S. Z. 1995. "On Discontinuity-Adaptive Smoothness Priors in Computer Vision." *IEEE Transactions on Pattern Analysis and Machine Intelligence* 17: 576–586. doi:10.1109/34.387504.
- Li, S. Z. 2009. *Markov Random Field Modeling in Image Analysis*. London: Springer. ISBN: 978-1-84800-279-1.
- Magnussen, S., P. Boudewyn, and M. Wulder. 2004. "Contextual Classification of Landsat TM Images to Forest Inventory Cover Types." *International Journal of Remote Sensing* 25 (12): 2421–2440. doi:10.1080/01431160310001642296.
- Mather, P., and B. Tso. 2010. *Classification Methods for Remotely Sensed Data*. London: CRC Press. ISBN: 9781420090727.
- Pontius, Jr. R. G., and M. L. Cheuk. 2006. "A Generalized Cross-Tabulation Matrix to Compare Soft-Classified Maps at Multiple Resolutions." *International Journal of Geographical Information Science* 20 (1): 1–30. doi:10.1080/13658810500391024.
- Silvan-Cardenas, J., and L. Wang. 2008. "Sub-Pixel Confusion Uncertainty Matrix for Assessing Soft Classifications." *Remote Sensing of Environment* 112 (3): 1081–1095. doi:10.1016/j.rse.2007.07.017.
- Singha, M., A. Kumar, A. Stein, P. N. L. Raju, and Y. K. Murthy. 2015. "Importance of DA-MRF Models in Fuzzy Based Classifier." *Journal of the Indian Society of Remote Sensing* 43 (1): 1–9.

- Tolpekin, V. A., and A. Stein. 2009. "Quantification of the Effects of Land-Cover-Class Spectral Separability on the Accuracy of Markov-Random-Field-Based Superresolution Mapping." *IEEE Transactions on Geoscience and Remote Sensing* 47 (9): 3283–3297. doi:[10.1109/TGRS.2009.2019126](https://doi.org/10.1109/TGRS.2009.2019126).
- Townsend, P. A. 2000. "A Quantitative Fuzzy Approach to Assess Mapped Vegetation Classifications for Ecological Applications." *Remote Sensing of Environment* 72 (3): 253–267. doi:[10.1016/S0034-4257\(99\)00096-6](https://doi.org/10.1016/S0034-4257(99)00096-6).
- Tso, B., and R. C. Olsen. 2005. "Combining Spectral and Spatial Information into Hidden Markov Models for Unsupervised Image Classification." *International Journal of Remote Sensing* 26 (10): 2113–2133. doi:[10.1080/01431160512331337844](https://doi.org/10.1080/01431160512331337844).
- Zadeh, L. A. 1965. "Fuzzy Sets." *Information and Control* 8 (3): 338–353. doi:[10.1016/S0019-9958\(65\)90241-X](https://doi.org/10.1016/S0019-9958(65)90241-X).
- Zhang, J., and G. Foody. 1998. "A Fuzzy Classification of Sub-Urban Land Cover from Remotely Sensed Imagery." *International Journal of Remote Sensing* 19 (14): 2721–2738. doi:[10.1080/014311698214479](https://doi.org/10.1080/014311698214479).